Letter

Thermal Ising transition in two-dimensional SU(3) Fermi lattice gases with population imbalance

Hayato Motegi,[1] Giacomo Marmorini,[1,2] Nobuo Furukawa,[1] and Daisuke Yamamoto[2,*]

[1]*Department of Physics and Mathematics, Aoyama Gakuin University, Sagamihara, Kanagawa 252-5258, Japan*

[2]*Department of Physics, Nihon University, Tokyo 156-8550, Japan*

(Received 13 September 2022; revised 25 March 2023; accepted 17 May 2023; published 20 June 2023)

We focus on three-component SU(3) Fermi gases loaded into a square optical lattice, with population imbalance between one component and the others. At strong coupling the system is described by the SU(3) Heisenberg model with an external field that couples to the population imbalance. We discuss the ground state at the mean-field level and then analyze the thermal fluctuations with the semiclassical Monte Carlo method. The interplay of interactions, population imbalance, and thermal fluctuations gives rise to a phase transition linked to the breaking of an emergent Ising symmetry, despite the absence of frustration. This represents another scenario of discrete symmetry breaking in low-dimensional systems with continuous symmetries. Possible implementations with cold alkaline-earth(-like) atoms are discussed.

DOI: 10.1103/PhysRevResearch.5.L022056

Introduction. Symmetry and its spontaneous breaking have been playing a central role for understanding the low-energy physics of many-body systems and classifying phase transition phenomena. According to the Mermin-Wagner-Hohenberg theorem [1,2], continuous symmetries cannot be spontaneously broken at nonzero temperature in one- and two-dimensional systems with sufficiently short-range interactions. However, it has been found in certain systems with only continuously symmetric interactions that a spontaneous symmetry breaking with respect to a discrete order parameter can emerge through a nontrivial mechanism even in low dimensions at nonzero temperature. In the framework of Heisenberg-like models, in a seminal work [3], Chandra, Coleman, and Larkin introduced the idea that this scenario can be realized in the presence of frustration coming from competing exchange interactions; in fact, their proposal of an Ising transition in the frustrated J_1-J_2 model on the square lattice has been confirmed in various subsequent studies [4–6]. An additional example of this kind is given by the Ising transition in the fully frustrated spin-1/2 Heisenberg ferromagnetic/antiferromagnetic square bilayer, which exhibits a finite-temperature phase transition in the two-dimensional (2D) Ising universality class [7,8], occurring at the endpoint of the discontinuous (first-order) phase transition between the singlet-dimer and fully polarized triplet phases. In the triangular lattice Heisenberg model it is the interplay of geometric frustration and magnetic field that stabilizes the up-up-down state, which breaks only a discrete translational Z_3 symmetry. In this Letter we aim to extend these concepts to SU($\mathcal{N}$)-symmetric Heisenberg models: We argue that, even without frustration coming from geometry or competing exchange interactions, the presence of a suitable "external field" [the SU($\mathcal{N}$) symmetry admits $\mathcal{N}-1$ couplings that play the role of generalized magnetic fields] can indeed induce the breaking of an emergent discrete symmetry.

The optimal experimental platform to test the above idea is given by ultracold atoms in optical lattices, which represent invaluable quantum simulators of many-body physics. For instance, two-component Fermi atoms in an optical lattice can realize the Hubbard model [9], the simplest model for strongly correlated electrons. At half filling and strong coupling the system is well approximated by the SU(2) Heisenberg model [10], and recent experiments employing the quantum gas microscope technique have confirmed that in a square optical lattice short-range spin-spin correlations exhibit finite correlation length, as expected at low but finite temperatures ($\gtrsim$0.25 times the tunneling energy) [9]. Owing to the advances in the manipulation of cold alkaline-earth(-like) atoms, such as ^{173}Yb and ^{87}Sr, analogous experiments on systems with SU($\mathcal{N}$) symmetry, $\mathcal{N}>2$, have been underway [11–14]. This has stimulated vast theoretical work, leading to numerous predictions of exotic ground states for various lattice geometries and and degrees $\mathcal{N}$ [15–19]. However, the effects of "external fields" that partially break the SU($\mathcal{N}$) symmetry have been rarely investigated, as well as those of thermal fluctuations [20]. Note that in cold-atom experiments, such an external-field effect can be simulated by imposing a global imbalance of populations among the $\mathcal{N}$ components [21].

Model. Inspired by the previous considerations, in this Letter we study the strong-coupling regime of three-component Fermi gases with SU(3)-symmetric interactions in a square optical lattice at 1/3 filling [15,16] with population imbalance between one component and the others, which breaks the original SU(3) symmetry down to SU(2) × U(1). The system is described by the antiferromagnetic SU(3) Heisenberg model

*Corresponding author: yamamoto.daisuke21@nihon-u.ac.jp

Published by the American Physical Society under the terms of the Creative Commons Attribution 4.0 International license. Further distribution of this work must maintain attribution to the author(s) and the published article's title, journal citation, and DOI.

with an external field,

$$\hat{\mathcal{H}} = \frac{J}{2}\sum_{\langle i,j\rangle}\hat{\boldsymbol{\lambda}}_i\cdot\hat{\boldsymbol{\lambda}}_j - D\sum_i \hat{\lambda}_{8,i} \quad (J>0), \tag{1}$$

where $\hat{\boldsymbol{\lambda}}_i = (\hat{\lambda}_{1,i}, \hat{\lambda}_{2,i}, \ldots, \hat{\lambda}_{8,i})$ are the generators of the SU(3) Lie algebra in the defining representation [22], acting on the three local basis states, which we refer to as three "colors," $|\mathrm{R}_i\rangle$, $|\mathrm{B}_i\rangle$, and $|\mathrm{G}_i\rangle$ [15,16], at site i. In the form given by the Gell-Mann matrices, $\hat{\lambda}_3$ and $\hat{\lambda}_8$ are diagonal, $\mathrm{diag}[1,0,-1]$ and $\frac{1}{\sqrt{3}}\mathrm{diag}[1,1,-2]$, respectively, while the others have off-diagonal entries, responsible for the color change of the local state. The last term of Eq. (1) represents a bias field controlling global population imbalance P_g between $\{\mathrm{R},\mathrm{B}\}$ and G. Although this partially breaks the original SU(3), the system still possesses the continuous SU(2) × U(1) symmetry, related to the global rotations in the SU(2) space generated by $\hat{\lambda}_{1-3}$ and that around $\hat{\lambda}_8$.

The SU(3) Heisenberg model corresponds to the spin-1 Hamiltonian with equal bilinear and biquadratic exchange couplings [23], which has been discussed in the context of spin liquid in $NiGa_2S_4$ [24], under the identifications $\{|\mathrm{R}_i\rangle, |\mathrm{B}_i\rangle, |\mathrm{G}_i\rangle\} \mapsto \{|1_i\rangle, |-1_i\rangle, |0_i\rangle\}$. In the language of solid state physics, the imbalance field D corresponds to the intrinsic single-ion anisotropy of the magnetic material. In artificial quantum systems of alkaline-earth(-like) atoms in optical lattices, the Hamiltonian (1) can be realized more directly with no fine tuning of coupling parameters. Those atoms possess SU($2I+1$)-symmetric repulsive interaction for nuclear spin I ($I = 5/2$ for ^{173}Yb and $I = 9/2$ for ^{87}Sr), and the technique of optical pumping allows for the preparation of any number $\mathcal{N}$ of components out of the $2I+1$ spin states [25].

The mean-field ground state. First, we consider the mean-field ground state of Eq. (1) at zero temperature, based on a variational wave function of the form $|\Psi\rangle = \prod_i |\psi_i\rangle$ with $|\psi_i\rangle = d_{\mathrm{R},i}|\mathrm{R}_i\rangle + d_{\mathrm{B},i}|\mathrm{B}_i\rangle + d_{\mathrm{G},i}|\mathrm{G}_i\rangle$. The coefficients can be represented by a normalized complex vector parametrized as

$$\begin{aligned}\boldsymbol{d}_i &\equiv (d_{\mathrm{R},i}, d_{\mathrm{B},i}, d_{\mathrm{G},i}) \\ &= \left(\sqrt{s_i}\cos\frac{\theta_i}{2}, \sqrt{s_i}e^{i\phi_i}\sin\frac{\theta_i}{2}, e^{i\alpha_i}\sqrt{1-s_i}\right).\end{aligned} \tag{2}$$

The amplitude and phases $(s_i,\theta_i,\phi_i,\alpha_i) \in [0,1]\times[0,\pi]\times[0,2\pi)^2$ should be determined in such a way that the variational energy $E_\mathrm{MF} = \langle\Psi|\hat{\mathcal{H}}|\Psi\rangle = J\sum_{\langle i,j\rangle}|\boldsymbol{d}_i^\dagger\cdot\boldsymbol{d}_j|^2 - D\sum_i(3s_i-2)/\sqrt{3}$ is minimized. For $D=0$, namely at the SU(3)-symmetric point, the minimization only imposes that the $\boldsymbol{d}_i$ vectors on neighboring sites are orthogonal. This is not enough to uniquely determine the global configuration of the $\boldsymbol{d}_i$ vectors, resulting in an accidental ground-state degeneracy within the mean-field approximation. Previous studies have predicted that the thermal fluctuations favor the Néel configuration shown in Fig. 1(a) via entropic selection [15,16], while the three-color stripe long-range order shown in Fig. 1(b) is chosen via a quantum order by disorder mechanism.

In the presence of an imbalance field D, this degeneracy is already lifted without taking fluctuations into account. In Figs. 1(c) and 1(d), we show the values of the energy per site and the global population imbalance P_g, respectively, as functions of D/J, for several mean-field solutions, labeled

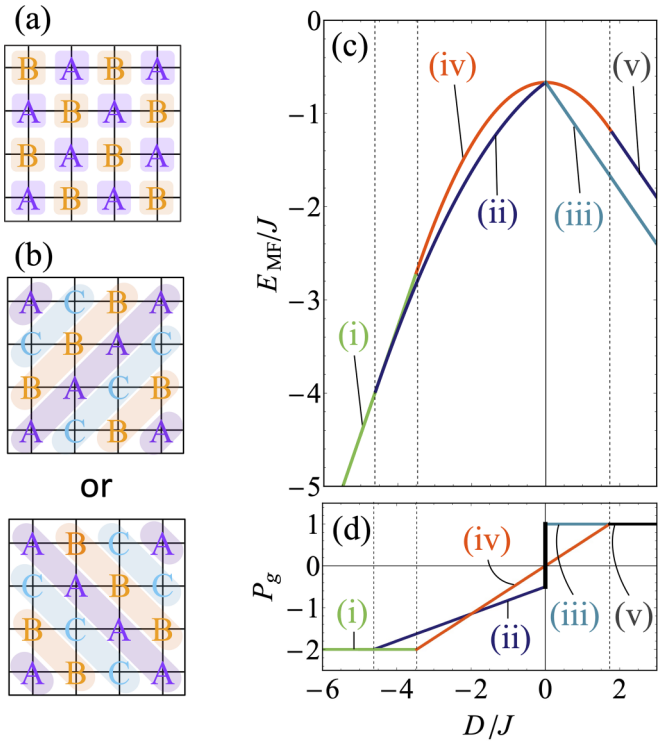


FIG. 1. Illustration of the two- and three-sublattice structures with ordering wave vectors (a) $\boldsymbol{Q}_2 = (\pi,\pi)$ and (b) $\boldsymbol{Q}_3^- = (2\pi/3, -2\pi/3)$ or $\boldsymbol{Q}_3^+ = (2\pi/3, 2\pi/3)$. Sublattices are labeled A, B, C. (c) Energy per site and (d) global population imbalance of the mean-field states as functions of the field D at zero temperature.

(i)–(v). For $D<0$, the imbalance field D tends to increase the global population of the $|\mathrm{G}\rangle$ state and competes with the antiferromagnetic coupling J, which tends to arrange different colors at neighboring sites. When D is sufficiently negative ($D < -8J/\sqrt{3}$), the forced ferromagnetic state [(i) in Fig. 1] is formed ($|\psi_i\rangle = |\mathrm{G}\rangle$ for all i). For $-8J/\sqrt{3} < D < 0$, we found the "minority-united canted-Néel" (MUCN) phase [(ii) in Figs. 1 and 2], in which the variational parameters in Eq. (2) are $(s_i,\theta_i,\phi_i,\alpha_i) = [\frac{1}{2}(1+\frac{\sqrt{3}}{8}\frac{D}{J}), \theta_0, \phi_0, \boldsymbol{Q}_2\cdot\boldsymbol{r}_i + \alpha_0]$, as the ground state. Here, the phases θ_0, ϕ_0, and α_0 are arbitrary and $\boldsymbol{Q}_2 = (\pi,\pi)$ is the propagation vector. In the MUCN state, while the phase α_i is alternating on the two sublattices [see Fig. 1(a)], interestingly the SU(2) sector of R and B exhibits ferromagnetic order with uniform θ_0 and ϕ_0, despite the antiferromagnetic nature of the exchange interaction. This can be understood as a mechanism to minimize the interaction energy between the majority G and the minorities $\{\mathrm{R},\mathrm{B}\}$. Notice that the MUCN state can be mapped to the conventional canted-Néel state of quantum antiferromagnets under magnetic field through the mapping $\cos(\theta/2)|\mathrm{R}\rangle + e^{i\phi}\sin(\theta/2)|\mathrm{B}\rangle \mapsto |\uparrow\rangle$, $|\mathrm{G}\rangle \mapsto |\downarrow\rangle$. For $D>0$, since the global population of $\{|\mathrm{R}_i\rangle, |\mathrm{B}_i\rangle\}$ tends to increase, there is no competition with the antiferromagnetic interactions. Therefore, an infinitesimally small field stabilizes (iii), the standard Néel order (with R and B), which is of course the ground state of the SU(2) Heisenberg model.

Although the mean-field theory predicts the two-sublattice ground states (MUCN and R-B Néel), besides the uniform

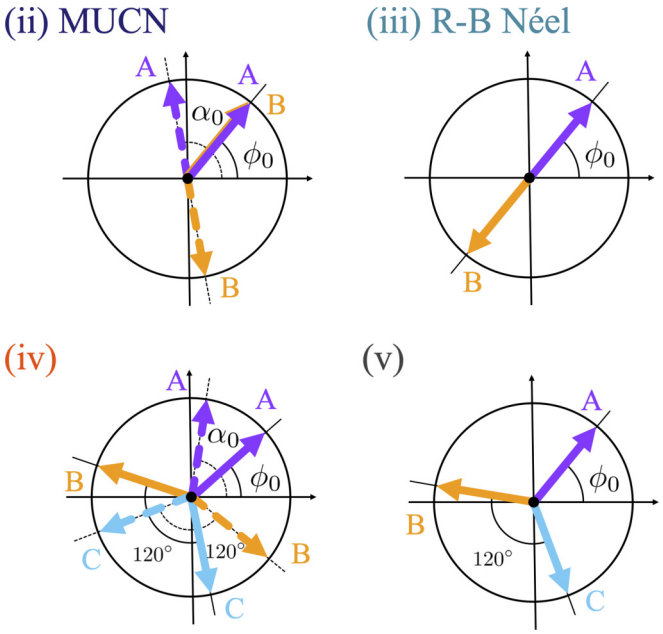


FIG. 2. Two relative phases α_i, ϕ_i in the mean-field states (ii)–(iv) on the corresponding sublattice structures displayed in Figs. 1(a) or 1(b) in a fixed gauge with $\theta_i = \pi/2$. The angles α_0, ϕ_0 can be arbitrarily chosen independently. In states (iii) and (v), α_i is not defined since $s_i = 1$.

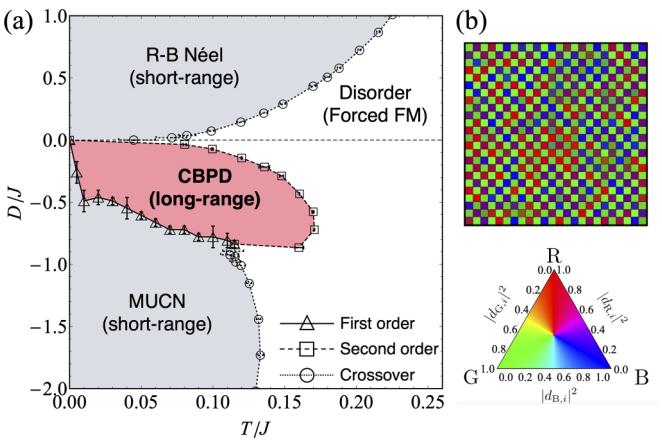


FIG. 3. (a) Thermal phase diagram obtained by the sMC simulations. The crossover temperature T_c^* is determined by the temperature where the correlation length reaches ten sites. (b) A snapshot of the checkerboard partially disordered state (CBPD) order from the Monte Carlo simulations.

state for $D < -8J/\sqrt{3}$, we also found three-sublattice solutions as metastable states [corresponding to (iv) and (v) in Figs. 1(c) and 1(d)]. While in state (iv) the three colors coexist with $r(D<0) = \frac{1}{2}(1 + \frac{1}{\sqrt{3}}\frac{D}{J})$, $r(D>0) = \frac{1}{2}(1 - \frac{1}{2\sqrt{3}}\frac{D}{J})$, the component $|\mathrm{G}\rangle$ vanishes in state (v), that is, $s_i = 1$. All these states, including the above-mentioned MUCN and R-B Néel, are massively degenerate, owing to the SU(2) × U(1) symmetry of the Hamiltonian. Upon choosing the gauge $\theta_i = \pi/2$, for which densities of B and R particles are identical and uniform on the lattice, we summarize the remaining two parameters ϕ and α of the mean-field solutions [(ii)–(v)] in Fig. 2.

Thermal phase diagram. Since the lowest temperatures reached in current experiments are in the range $T \simeq 0.7J$ [SU(6) chain] [12] to $T \simeq 0.9J$ [SU(2) square lattice] [9], addressing the finite-temperature effects becomes important beyond a purely theoretical motivation. We hereby take into account thermal fluctuations from the mean-field ground state using semiclassical multicolor Monte Carlo (sMC) simulations [20,26,27].

We perform the standard Metropolis algorithm that allows the complex vectors $\boldsymbol{d}_i$ on $L \times L$ sites under periodic boundary conditions to fluctuate thermally with the Boltzmann weight $\exp(-E_{\mathrm{MF}}/T)$. In addition, we employ the relaxation acceleration (RA) technique [20] with local unitary transformations $\exp(ic\hat{\mathcal{H}}_i^{\mathrm{loc}}/\|\hat{\mathcal{H}}_i^{\mathrm{loc}}\|_{\mathrm{F}})$ defined by the local mean-field Hamiltonian $\hat{\mathcal{H}}_i^{\mathrm{loc}} = \frac{J}{2}\sum_{j\in \mathrm{NN}_i}\langle\hat{\boldsymbol{\lambda}}_j\rangle \cdot \hat{\boldsymbol{\lambda}}_i - D\hat{\lambda}_{8,i}$. Here, the real number c is randomly generated from an uniform distribution on the interval $[-1, 1]$, $\|\cdots\|_{\mathrm{F}}$ is the Frobenius norm, and the sum runs over all nearest-neighbor sites of site i. In the case of the SU(3) system, the eigenvalues of $\hat{\mathcal{H}}_i^{\mathrm{loc}}$ can be calculated analytically, which contributes to the reduction of the calculation cost [28]. The single Monte Carlo step consists of the Metropolis updates for $d_{\sigma,i}$ over the entire lattice, followed by double RA sweeps. This procedure can enhance decorrelation and increase the convergence speed [20].

Figure 3 shows the sMC thermal phase diagram. The most surprising feature is a fluctuation-induced phase with true long-range order emerging for $-0.8 \lesssim D < 0$. The R-B Néel and MUCN states, being continuous-symmetry-breaking states, only possess short-range correlations and a crossover connects them to the high-temperature disordered phase.

In order to determine the transition (or crossover) lines in Fig. 4, we calculate the correlation lengths [20,29] $\xi(\boldsymbol{q}) = |\delta\boldsymbol{q}|^{-1}\sqrt{[\mathcal{S}(\boldsymbol{q})/\mathcal{S}(\boldsymbol{q}+\delta\boldsymbol{q})] - 1}$, where $\mathcal{S}(\boldsymbol{q})$ is the structure factor for wave vector $\boldsymbol{q}$ and $\delta\boldsymbol{q} = (2\pi/L, 0)$. We use $\mathcal{S}^{\mathrm{SU}(2)}(\boldsymbol{q}) = \sum_{\mu=1}^{3}\langle|\sum_i \hat{\lambda}_{\mu,i}e^{i\boldsymbol{q}\cdot\boldsymbol{r}_i}|^2/L^2\rangle$ and $\mathcal{S}^{\mathrm{U}(1)}(\boldsymbol{q}) = \langle|\sum_i \hat{\lambda}_{8,i}e^{i\boldsymbol{q}\cdot\boldsymbol{r}_i}|^2/L^2\rangle$ to detect the correlations in the SU(2) and U(1) sectors, respectively. The R-B Néel and MUCN phases can be identified by $\mathcal{S}^{\mathrm{SU}(2)}(\boldsymbol{q})$ with ordering vectors $\boldsymbol{q} = \boldsymbol{Q}_2 \equiv (\pi, \pi)$ and $\boldsymbol{q} = \boldsymbol{0}$, respectively. We confirm that there is no crossing point of $\xi^{\mathrm{SU}(2)}/L$ for different system sizes down to low temperatures [see a typical case in Fig. 4(a)], which indicates no long-range order at $T > 0$ as expected. In Fig. 3, we plot the crossover temperature T_c^* from disordered to short-range correlated state by choosing the condition $\xi^{\mathrm{SU}(2)} = 10$ sites [see Fig. 4(b)], which is comparable to the linear system size in typical cold-atom experiments in two dimensions [9].

The emergence of the nontrivial true long-range order between the regions with the R-B Néel and MUCN short-range correlations for $T > 0$ is of particular significance. In this phase, most of the snapshots in the sMC simulations show a checkerboard pattern where one sublattice is occupied mostly by $|\mathrm{G}\rangle$ and the other by random superpositions of $|\mathrm{R}\rangle$ and $|\mathrm{B}\rangle$: $|\psi_{i_\mathrm{A}}\rangle \simeq |\mathrm{G}\rangle$, $|\psi_{i_\mathrm{B}}\rangle \simeq \cos(\theta_{i_\mathrm{B}}/2)|\mathrm{R}_{i_\mathrm{B}}\rangle + e^{i\phi_{i_\mathrm{B}}}\sin(\theta_{i_\mathrm{B}}/2)|\mathrm{B}_{i_\mathrm{B}}\rangle$, where $\theta_{i_\mathrm{B}}, \phi_{i_\mathrm{B}}$ are randomly chosen at each site in each sMC snapshot [i.e., disordered in the SU(2) sector]. This state breaks neither SU(2) nor U(1) symmetry, but *only the discrete translational symmetry*. Thus, the

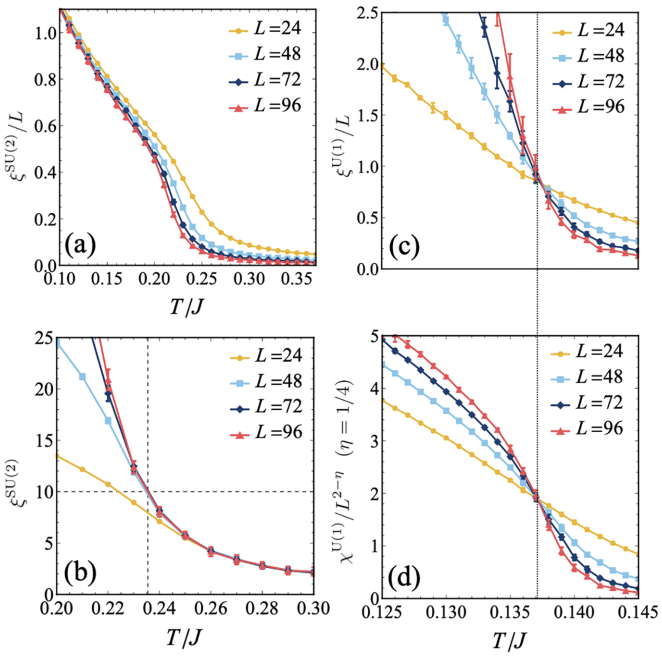


FIG. 4. Typical examples of the numerical data for the scaling analyses that obtain the finite-temperature phase diagram shown in Fig. 3. (a) Scaled correlation length $\xi^{\mathrm{SU}(2)}/L$ and (b) correlation length $\xi^{\mathrm{SU}(2)}$ along $D/J = 2/\sqrt{3}$. (c) Scaled correlation length and (b) scaled spin susceptibility with respect to $\hat{\lambda}_8$ at $D/J = -1/2\sqrt{3}$.

Mermin-Wagner-Hohenberg theorem [1,2] does not forbid a finite-temperature phase transition to this checkerboard partially disordered state (CBPD) with true long-range order. In fact, as seen in Fig. 4(c), the scaled correlation lengths $\xi^{\mathrm{U}(1)}/L$, obtained from $\mathcal{S}^{\mathrm{U}(1)}(\boldsymbol{q} = \boldsymbol{Q}_2)$, for different linear sizes L cross each other at a certain critical point $T_{\mathrm{c}} > 0$. According to the finite-size scaling theory the scaled magnetic susceptibility $\chi^{\mathrm{U}(1)}/L^{2-\eta}$, where $\chi^{\mathrm{U}(1)} = (J/k_{\mathrm{B}}T)\mathcal{S}^{\mathrm{U}(1)}(\boldsymbol{Q}_2)$, should become size independent at the critical temperature T_{c}: Fig. 4(d) shows that this scaling law is reproduced with critical exponent $\eta = 1/4$, indicating the 2D Ising universality class, as expected from the Z_2 translational symmetry breaking of the checkerboard pattern.

Let us discuss the mechanism of the emergence of CBPD order. Within the mean-field approximation, this phase is included in the infinitely degenerate ground-state manifold at the SU(3)-symmetric point, since each pair of the $\boldsymbol{d}_i$ vectors on neighboring sites is orthogonal. For $T > 0$ one sublattice is disordered in the SU(2) sector while the checkerboard pattern is kept. Since the partial disorder compensates the loss of entropy, thermal fluctuations select this phase from the zero-temperature degenerate manifold [30]. Let us also recall that the three-sublattice state selected by purely quantum fluctuations is unstable for any $T > 0$, according to linear flavor-wave theory [15], in favor of two-sublattice states, and therefore the CBPD phase is expected to be robust against the inclusion of quantum effects beyond single site. in the three-dimensional case, the entropic selection of two-sublattice phases has also been reported [18], although the three-sublattice phase is not completely excluded near zero temperature due to the higher dimensionality.

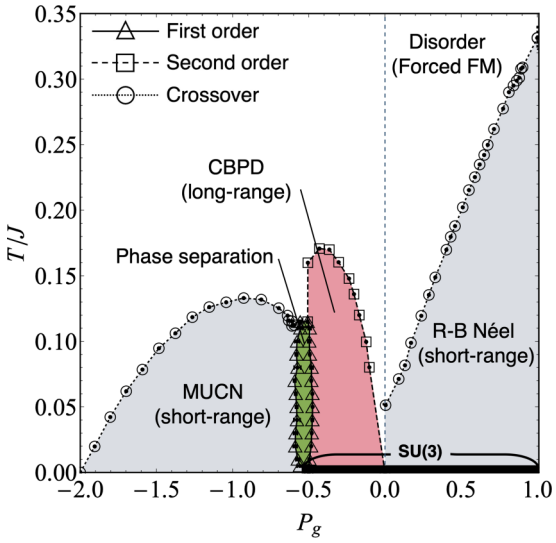


FIG. 5. Thermal phase diagram as a function of the population imbalance P_{g}. The thick horizontal line corresponds to the SU(3)-symmetric point. Along that line, the variational solution is highly degenerate.

Experimental detection. From an experimental perspective, it is convenient to describe the thermal phase diagram (Fig. 3) as a function of the global population imbalance P_{g} defined by $P_{\mathrm{g}} = \sqrt{3}\sum_i \langle\hat{\lambda}_{8,i}\rangle = \frac{N_{\mathrm{R}}+N_{\mathrm{B}}-2N_{\mathrm{G}}}{N_{\mathrm{R}}+N_{\mathrm{B}}+N_{\mathrm{G}}}$, where N_μ represents the global population of color μ [21], because this quantity, rather than D, is controllable in cold-atom experiments [21]. Figure 5 shows the T-P_{g} phase diagram. Note that a phase separation region appears between CBPD and MUCN. The detection of the CBPD order may be realized as follows. First, the $|\mathrm{G}\rangle$ state is removed from the entire lattice via optical pumping [25] and horizontal pairs of neighboring lattice sites are merged into single sites so as to form a new square lattice. We then look for signatures of the Mott insulating state, in which ideally all sites are singly occupied by either R or B state, with the established techniques [31–33]. The experiment is repeated and the same protocol is operated with vertical pairs instead. If, in both instances, the Mott insulating state is detected, this would be proof of the realization of the CBPD order. In addition, the eventual extension of the quantum gas microscope technique to SU($\mathcal{N}$) systems [34] could detect each phase more directly. Note that the sMC method replaces the statistics of discrete quantum levels by approximate continuous classical statistics of the vectors $\boldsymbol{d}_i$. Since this treatment should overestimate the entropy of paramagnetic states, thus underestimating the transition/crossover temperatures, the lines of $T_{\mathrm{c}}(T_{\mathrm{c}}^*)$ in Fig. 5 should be taken as lower bounds.

Conclusion. We have investigated the emergence of long-range order by thermal disorder in the square-lattice SU(3) Fermi gas at strong coupling with population imbalance and proposed experimental setups to realize and detect our predictions with alkaline-earth(-like) atoms. Applying mean-field theory and the sMC method to the SU(3) Heisenberg model, we found that the competition between antiferromagnetic interactions and the population imbalance gives rise to several interesting magnetic states, including a true long-range

ordered state that breaks only a discrete symmetry. This state enjoys an entropic advantage coming from the abundance of color degrees of freedom and is therefore favored by thermal fluctuations. This scenario generalizes the idea of emergent discrete symmetry breaking in low-dimensional systems without the traditional forms of magnetic frustration. Furthermore, we recall that the quantum fluctuations at $D = 0$ (no population imbalance) select the three-color stripe order, which should then persist for sufficiently small $D < 0$. This creates the condition for a finite-temperature transition originating from the difference between quantum and thermal order-by-disorder selection, a very rare phenomenon in magnetic systems [35,36].

In conclusion, our work offers other directions in SU($\mathcal{N} > 2$) magnetism, which is presently under intensive investigation in cold-atom experiments, showing further examples of the rich physics induced by population imbalance. It also provides more insight into the phase transition phenomena of highly symmetric systems, which can prove beneficial in other contexts, such as solid-state physics [24].

Acknowledgments. We would like to thank Y. Takahashi, Y. Takasu, and S. Taie for useful discussions. This work was supported by JSPS KAKENHI Grants No. 18K03525 (D.Y.), No. 21H05185 (G.M., D.Y.), No. 22H01171 (N.F., D.Y.), and JST PRESTO Grant No. JPMJPR2118, Japan (D.Y.).

[1] P. C. Hohenberg, Existence of long-range order in one and two dimensions, Phys. Rev. **158**, 383 (1967).

[2] N. D. Mermin and H. Wagner, Absence of Ferromagnetism or Antiferromagnetism in One- or Two-Dimensional Isotropic Heisenberg Models, Phys. Rev. Lett. **17**, 1133 (1966).

[3] P. Chandra, P. Coleman, and A. I. Larkin, Ising Transition in Frustrated Heisenberg Models, Phys. Rev. Lett. **64**, 88 (1990).

[4] C. Weber, L. Capriotti, G. Misguich, F. Becca, M. Elhajal, and F. Mila, Ising Transition Driven by Frustration in a 2D Classical Model with Continuous Symmetry, Phys. Rev. Lett. **91**, 177202 (2003).

[5] L. Capriotti, A. Fubini, T. Roscilde, and V. Tognetti, Ising Transition in the Two-Dimensional Quantum J_1-J_2 Heisenberg Model, Phys. Rev. Lett. **92**, 157202 (2004).

[6] O. Gauthé and F. Mila, Thermal Ising Transition in the Spin-$1/2$ $J_1 - J_2$ Heisenberg Model, Phys. Rev. Lett. **128**, 227202 (2022).

[7] K. Karľová and J. Strečka, Continuous field-driven phase transition from the Ising universality class of a frustrated spin-1/2 Heisenberg FM/AF square bilayer, Solid State Commun. **281**, 31 (2018).

[8] K. Karľová and J. Strečka, Ising-type critical exponents of the fully frustrated spin-1/2 Heisenberg FM/AF square bilayer at a critical magnetic field, Phase Transitions **92**, 317 (2019).

[9] A. Mazurenko, C. S. Chiu, G. Ji, M. F. Parsons, M. Kanász-Nagy, R. Schmidt, F. Grusdt, E. Demler, D. Greif, and M. Greiner, A cold-atom Fermi–Hubbard antiferromagnet, Nature (London) **545**, 462 (2017).

[10] H. Kawamura and S. Miyashita, Phase transition of the two-dimensional Heisenberg antiferromagnet on the triangular lattice, J. Phys. Soc. Jpn. **53**, 4138 (1984).

[11] C. Hofrichter, L. Riegger, F. Scazza, M. Höfer, D. R. Fernandes, I. Bloch, and S. Fölling, Direct Probing of the Mott Crossover in the SU(N) Fermi-Hubbard Model, Phys. Rev. X **6**, 021030 (2016).

[12] S. Taie, E. Ibarra-García-Padilla, N. Nishizawa, Y. Takasu, Y. Kuno, H.-T. Wei, R. T. Scalettar, K. R. A. Hazzard, and Y. Takahashi, Observation of antiferromagnetic correlations in an ultracold SU(N) Hubbard model, Nat. Phys. **18**, 1356 (2022).

[13] M. A. Cazalilla and A. M. Rey, Ultracold Fermi gases with emergent SU(N) symmetry, Rep. Prog. Phys. **77**, 124401 (2014).

[14] Y. Takahashi, Quantum simulation of quantum many-body systems with ultracold two-electron atoms in an optical lattice, Proc. Jpn. Acad., Ser. B **98**, 141 (2022).

[15] T. A. Tóth, A. M. Läuchli, F. Mila, and K. Penc, Three-Sublattice Ordering of the SU(3) Heisenberg Model of Three-Flavor Fermions on the Square and Cubic Lattices, Phys. Rev. Lett. **105**, 265301 (2010).

[16] B. Bauer, P. Corboz, A. M. Läuchli, L. Messio, K. Penc, M. Troyer, and F. Mila, Three-sublattice order in the SU(3) Heisenberg model on the square and triangular lattice, Phys. Rev. B **85**, 125116 (2012).

[17] P. Corboz, A. M. Läuchli, K. Penc, M. Troyer, and F. Mila, Simultaneous Dimerization and SU(4) Symmetry Breaking of 4-Color Fermions on the Square Lattice, Phys. Rev. Lett. **107**, 215301 (2011).

[18] A. Sotnikov and W. Hofstetter, Magnetic ordering of three-component ultracold fermionic mixtures in optical lattices, Phys. Rev. A **89**, 063601 (2014).

[19] M. Hafez-Torbati and W. Hofstetter, Competing charge and magnetic order in fermionic multicomponent systems, Phys. Rev. B **100**, 035133 (2019).

[20] D. Yamamoto, C. Suzuki, G. Marmorini, S. Okazaki, and N. Furukawa, Quantum and Thermal Phase Transitions of the Triangular SU(3) Heisenberg Model under Magnetic Fields, Phys. Rev. Lett. **125**, 057204 (2020).

[21] P. T. Brown, D. Mitra, E. Guardado-Sanchez, P. Schauß, S. S. Kondov, E. Khatami, T. Paiva, N. Trivedi, D. A. Huse, and W. S. Bakr, Spin-imbalance in a 2D Fermi-Hubbard system, Science **357**, 1385 (2017).

[22] M. Gell-Mann, Symmetries of baryons and mesons, Phys. Rev. **125**, 1067 (1962).

[23] A. Läuchli, F. Mila, and K. Penc, Quadrupolar Phases of the $S = 1$ Bilinear-Biquadratic Heisenberg Model on the Triangular Lattice, Phys. Rev. Lett. **97**, 087205 (2006).

[24] H. Tsunetsugu and M. Arikawa, Spin nematic phase in $S = 1$ triangular antiferromagnets, J. Phys. Soc. Jpn. **75**, 083701 (2006).

[25] S. Taie, Y. Takasu, S. Sugawa, R. Yamazaki, T. Tsujimoto, R. Murakami, and Y. Takahashi, Realization of a SU(2) × SU(6) System of Fermions in a Cold Atomic Gas, Phys. Rev. Lett. **105**, 190401 (2010).

[26] E. M. Stoudenmire, S. Trebst, and L. Balents, Quadrupolar correlations and spin freezing in $S = 1$ triangular lattice antiferromagnets, Phys. Rev. B **79**, 214436 (2009).

[27] K. Remund, R. Pohle, Y. Akagi, J. Romhányi, and N. Shannon, Semi-classical simulation of spin-1 magnets, Phys. Rev. Res. **4**, 033106 (2022).

[28] J. Kopp, Efficient numerical diagonalization of Hermitian 3×3 matrices, Int. J. Mod. Phys. C **19**, 523 (2008).

[29] L. Seabra, T. Momoi, P. Sindzingre, and N. Shannon, Phase diagram of the classical Heisenberg antiferromagnet on a triangular lattice in an applied magnetic field, Phys. Rev. B **84**, 214418 (2011).

[30] We conjecture that this argument should be true also for $\mathcal{N} > 3$, that is the SU($\mathcal{N}$) Heisenberg model with $-D\sum_i \hat{\lambda}_{\mathcal{N}^2-1,i}$ field term.

[31] R. Jördens, N. Strohmaier, K. Günter, H. Moritz, and T. Esslinger, A Mott insulator of fermionic atoms in an optical lattice, Nature (London) **455**, 204 (2008).

[32] J. F. Sherson, C. Weitenberg, M. Endres, M. Cheneau, I. Bloch, and S. Kuhr, Single-atom-resolved fluorescence imaging of an atomic Mott insulator, Nature (London) **467**, 68 (2010).

[33] D. Greif, L. Tarruell, T. Uehlinger, R. Jördens, and T. Esslinger, Probing Nearest-Neighbor Correlations of Ultracold Fermions in an Optical Lattice, Phys. Rev. Lett. **106**, 145302 (2011).

[34] D. Okuno, Y. Amano, K. Enomoto, N. Takei, and Y. Takahashi, Schemes for nondestructive quantum gas microscopy of single atoms in an optical lattice, New J. Phys. **22**, 013041 (2020).

[35] Q. Sheng and C. L. Henley, Ordering due to disorder in a triangular Heisenberg antiferromagnet with exchange anisotropy, J. Phys.: Condens. Matter **4**, 2937 (1992).

[36] D. Yamamoto, G. Marmorini, M. Tabata, K. Sakakura, and I. Danshita, Magnetism driven by the interplay of fluctuations and frustration in the easy-axis triangular XXZ model with transverse fields, Phys. Rev. B **100**, 140410(R) (2019).